Neutralized Drift Compression Experiments (NDCX) with a High Intensity Ion Beam

P. K. Roy[1*], S. S. Yu[1], W. L. Waldron[1], A. Anders[1], D. Baca[1], J. J. Barnard[2], F. M. Bieniosek[1], J. Coleman[1], R. C. Davidson[3], P. C. Efthimion[3], S. Eylon[1], A. Friedman[2], E. P. Gilson[3], W. G. Greenway[1], E. Henestroza[1], I. Kaganovich[3], M. Leitner[1], B. G. Logan[1], A. B. Sefkow[3], P. A. Seidl[1], W. M. Sharp[2], C. Thoma[4] and D. R. Welch[4]

[1]*Lawrence Berkeley National Laboratory, 1 Cyclotron Rd, Berkeley, California 94720, USA.*
[2]*Lawrence Livermore National Laboratory, Livermore, California 94550, USA.*
[3]*Princeton Plasma Physics Laboratory, New Jersey 08543-0451, USA.*
[4]*Voss Scientific, Albuquerque, NM 87108, USA.*
Elsevier use only: Received date here; revised date here; accepted date here

Abstract

To create high energy density matter and fusion conditions, high-power drivers, such as lasers, ion beams, and x-ray drivers, are employed to heat targets with pulses short compared to hydro-motion. Both high energy density physics and ion-driven inertial fusion require the simultaneous transverse and longitudinal compression of an ion beam to achieve high intensities. We have previously studied the effects of plasma neutralization for transverse beam compression. The scaled experiment, the Neutralized Transport Experiment (NTX), demonstrated that an initially un-neutralized beam can be compressed transversely to ~1 mm radius when charge neutralization by background plasma electrons is provided. Here we report longitudinal compression of a velocity-tailored, intense, neutralized 25 mA K^+ beam at 300 keV. The compression takes place in a 1-2 m drift section filled with plasma to provide space-charge neutralization. An induction cell produces a head-to-tail velocity tilt that longitudinally compresses the neutralized beam, enhances the beam peak current by a factor of 50 and produces a pulse duration of about 3 ns. The Physics of longitudinal compression, experimental procedure, and the results of the compression experiments are presented.

Keywords: Beam; ion; longitudinal compression; plasma; neutralization; diagnostics; induction cell;

1. Introduction

Intense ion beams of moderate energy offer an attractive approach to heating dense matter uniformly to extreme conditions, because their energy deposition is nearly classical and shock-free. High energy density physics and ion-driven inertial fusion require the simultaneous transverse and longitudinal compression of an ion beam to achieve high intensities. A beam of ~200 A (1 beam, 23 MeV Na+) with a 1-mm focal spot radius and pulse length of ~1 ns would be ideal as a driver for Warm Dense Matter experiments. These beam spot sizes and pulse lengths are achievable with beam neutralization and longitudinal compression in background plasma. In beam neutralization, electrons from a plasma or external source are entrained by the beam and neutralize the space charge sufficiently that the pulse focuses on the target in a nearly ballistic manner to a small spot. Several numerical and experimental articles on beam neutralization and transverse compression have been published elsewhere[1-6]. In neutralized drift compression, the beam is longitudinally compressed by imposing a linear head-to-tail velocity tilt that produces a pulse duration of several ns. Longitudinal compression of space-charge-dominated beams has been studied extensively in theory and simulations [7-12]. Longitudinal space-charge forces limit the beam compression ratio, the ratio of the initial to final current, to about ten in most applications. An experiment with five-fold compression has been reported [13]. Recent theoretical models and simulations predicted that much higher compression ratios (of order 100) can be achieved if the beam compression takes place in a plasma-filled drift region in which the space-charge forces of the ion beam are neutralized [14, 15]. Experimentally, we have reported 50-fold compression in a brief letter [16]. The physics and technical issues, fast diagnostics, experimental results on longitudinal beam compression are presented in this article.

2. Physics and technical issues

2.1. Velocity tailored voltage ramp and compression

Figure 1 shows a concept of longitudinal beam compression. A 300-keV beam with 25-mA current of 10-μs pulse length, Fig. 1(a), enters a neutralized drift section, where a tilt voltage waveform, Fig.1(b), decelerates and accelerates roughly 300 ns of the 10 μs pulse and compresses the beam to a pulse of a few nanoseconds as shown in Fig.1(c). In general, the beam is longitudinally compressed by a tailored voltage waveform, generated by an induction cell. A brief description of the cell is presented in Section 3.2. Once the selected part of the beam pulse enters into the tilt cell voltage ramp region, its head is decelerated and its tail accelerated. Thus, the tilt core applies a head-to-tail velocity tilt on the beam pulse segment and increases the current by decreasing the pulse duration. The longitudinal envelope equation for a beam with a parabolic profile without space charge can be expressed as [17]

$$\frac{d^2L}{dS^2} = \frac{16\varepsilon_z^2}{L^3}, \qquad (1.1)$$

where L is the bunch length, S is the axial distance and ε_z is 5 times the rms longitudinal emittance. The velocity tilt required to compress the beam to a "stagnation" point (where dL/ds=0) is given by

$$\frac{\Delta V^2}{V^2} = \frac{16\varepsilon_z^2}{L_0^2}\left[C^2 - 1\right] \simeq \frac{C^2}{\eta^2}\left\langle \frac{\delta p^2}{p^2} \right\rangle \qquad (1.2)$$

where ΔV is the velocity difference between the tail and head of the beam, C is the ratio of initial bunch length, L_0, to final bunch length L_f, $\left\langle \left(\delta p^2 / p^2\right) \right\rangle$ is the fractional mean square in the momentum spread, and η is the conversion factor from a tilt to an rms quantity (η=0.29 for a beam with constant line charge). The voltage ramp ΔV required to produce a velocity tilt satisfies $\Delta V / V = 2\left(\Delta v / v\right)$, where v is the axial velocity obtained from the relation $qV = \frac{1}{2} mv^2$. Here $qV =$ ion energy and q is the ion charge.

If the compressed pulse length is dominated by the longitudinal beam temperature T_l, the compressed pulse length is approximately given by

$$L_f = \frac{d}{v_l^2}\sqrt{\frac{2kT_l}{M}}, \qquad (1.3)$$

where v_l, d, M and k are the mean longitudinal beam velocity, drift length, ion mass and Boltzmann constant, respectively. Here T_l is an effective temperature including the effects of errors in the tilt waveform.

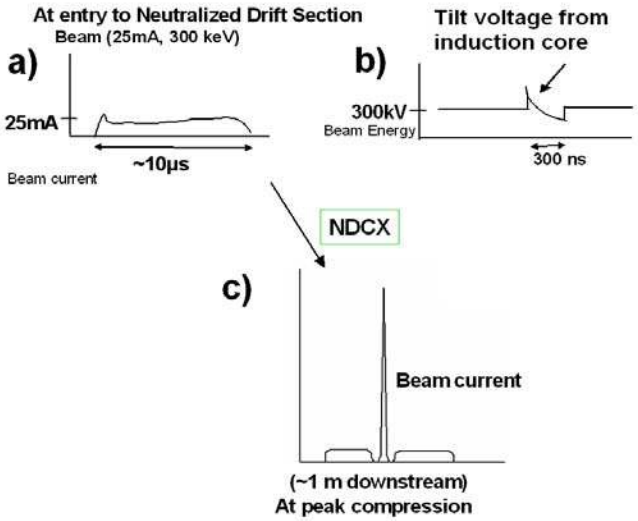

Fig. 1 : A sketch of the longitudinal current compression concept: (a) beam pulse before compression, (b) tilt core voltage waveform applied to uncompressed beam pulse, and (c) compressed beam current.

2.2. Plasma neutralization

The compressed beam bunch has higher space charge density than the uncompressed beam bunch section. This higher space charge can contribute to beam blow-up before reaching the target or diagnostic location. Therefore, the compressed beam must be neutralized with an appropriate plasma density. Typically, $n_p / Zn_b > 1$, where n_p is the plasma density, and n_b and Z are the ion beam density and charge state. This plasma neutralization is provided by co-moving electrons in the beam drift section filled with plasma, referred to here as the plasma column.

3. Experiment setup and diagnostics

The NDCX device consists of four major sections: a potassium source chamber with 300 keV Marx, a magnetic transport section with four pulsed quadrupoles, a velocity tailored voltage tilt cell, and a meter long plasma column with plasma plug, and beam diagnostics. Figure 2(a) shows a sketch of the NDCX layout, and Fig. 2(b) shows a photograph of the NDCX beamline. Major sections of the NDCX device are described in the following sub-sections.

3.1. Ion source, Marx and quadrupoles

The K^+ beam is produced on a standard hot-plate source, with the perveance being determined by passing the beam through a metal aperture after the diode. The NDCX experiment uses the same front end as the earlier Neutralized Transport Experiments (NTX) [1-6]. It consists of a 300 keV, 25-milliamp K^+ beam powered by a Marx generator. A timed crowbar switch produces pulses with a 10 μs flat-top. The four pulsed quadrupoles magnets used in NTX to control the beam envelope (beam radius and convergence angle) are retained for the present experiments on NDCX.

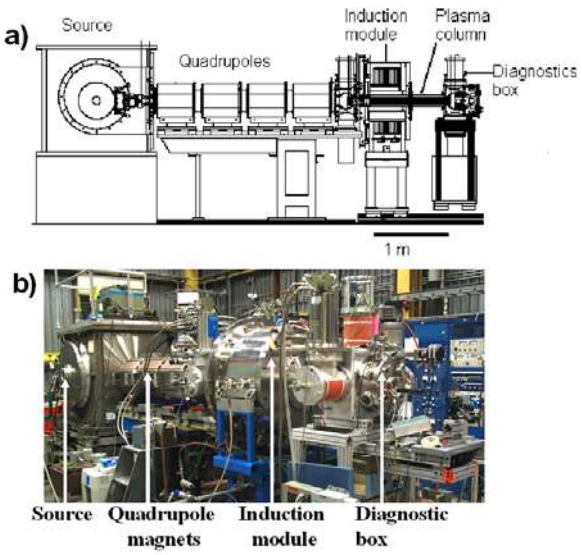

Fig.2: (a) A sketch of the NDCX beamline, and (b) photograph of the NDCX experimental setup.

3.2. Tilt cell

The induction module consists of 14 independently-driven ferromagnetic cores in a pressurized gas (SF_6) region that is separated from the vacuum by a conventional high voltage insulator. The basic concept of the induction cell is shown in Fig. 3. A pulsed voltage generates a changing magnetic field inside a ferromagnetic core. This change in magnetic flux inside the core induces an electric field along its axis, according to Faraday's law. The voltage pulse is timed so that the field is present when beam particles pass through the core. The waveforms applied to the 14 cores inductively add at the acceleration gap. Each core is driven by a thyratron-switched modulator. Because the modulator for each core can be designed to produce different waveforms and can be triggered independently, a variety of waveforms can be produced at the acceleration gap using the 14 discrete building blocks. The induction tilt voltage carves out a ~300 ns segment of the flat-top which compresses longitudinally as it drifts through a one-meter long plasma column.

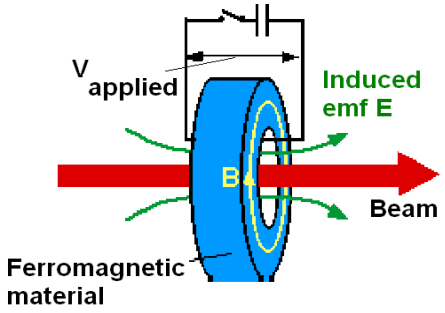

Fig. 3: Schematic of an induction accelerator module.

3.3. .Plasma source and plasma column

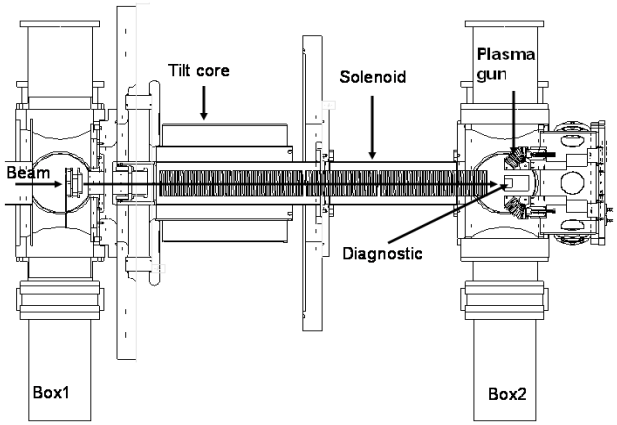

Fig.4: A sketch of compression and neutralization section.

Figure 4 shows a sketch of the plasma source and meter long plasma column with the induction module (tilt core). In this NDCX experiment, the plasma column is formed by two pulsed aluminum cathodic arc sources located at the downstream end. Each source is equipped with a 45^0 open-architecture macroparticle filter providing a flow of fully ionized aluminum plasma [18]. The two plasma flows are pointed at an angle of 45^0 towards the solenoidal column (~1kG, 7.6 cm diameter, and 1 m long). A significant fraction (>10%) of the plasma enters the solenoid, and drifts practically unattenuated through the entire column (the rest of the aluminum plasma condenses at the wall and is thereby removed from the system). In most of the operating regimes, the plasma density (> $5x10^{10}$ cm^{-3}) is at least a factor of 10 higher than the beam density and is maintained throughout the channel. Figure 5 shows the axial plasma density along the length of the plasma column for a plasma source (gun) [19]. A plasma density of 3 x

10^{11} to 5 x 10^{11} cm^{-3} is measured experimentally for two plasma guns and used in the experiment. At the upstream end of the column, we have introduced a plasma stopper consisting of two opposing magnetic dipoles of ~1kG each, which inhibit the motion of plasma upstream into the induction gap and the quadrupole focusing sections. A second plasma column consisting of a meter-long ferro-electric plasma source that does not require solenoidal confinement has been constructed and is undergoing experimental tests.

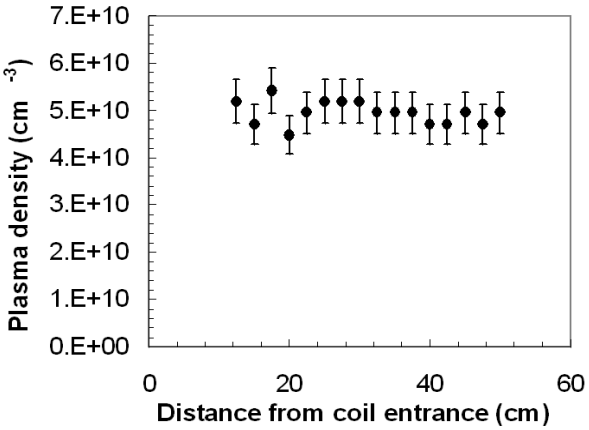

Fig.5: Variation of plasma density along the z-axis into the plasma channel for one plasma source (gun). Experimentally we have used two plasma guns.

3.4. Diagnostics

Figure 6 shows the diagnostics that are used in the experiment. The diagnostics are a moveable pinhole Faraday cup, and a moveable scintillator, the signal of which is detected using a gated camera or a phototube through a quartz glass window (>90% transmission wavelength between 300 to 100 nm). A brief description of each of these diagnostics is presented below.

3.4.1. Phototube diagnostic

A phototube diagnostic [20], Fig. 6(a), is used to measure beam pulse compression with and without neutralization. The optical system is based on a Hamamatsu phototube with fast (sub-ns) response which is coupled to a 500-MHz oscilloscope. The beam pulse is measured by using the phototube to collect the optical photon flux from an aluminum oxide scintillator placed in the path of the beam, Fig. 6(c). The time response of the scintillator is fast enough to make measurements on a nanosecond time scale. Small amounts of stray light emitted by the plasma over long periods of time (100s of μs) can drain the bias charge in the phototube's internal power supply, and thus spoil the gain of the phototube during the beam pulse. This background plasma light is blocked from entering the phototube by an electro-optic gated shutter (Displaytech) that opens just before the beam pulse arrives at the scintillator. The scintillator itself is not sensitive to low-energy plasma electrons. As a result, we have been able to obtain beam pulse compression data with minimal interference from the neutralizing plasma. Scintillator degradation over many beam pulses limits useful scintillator lifetime that has required vigilance.

A time-gated camera is also used to measure the beam optical profile and intensity. It has a time resolution of about 1 ns.

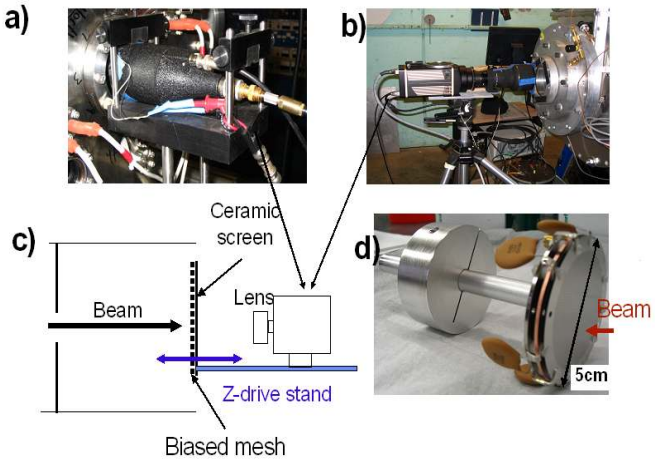

Fig.6: NDCX diagnostics: (a) a phototube, (b) a gated camera, (c) an assembly of the scintillator for the phototube and the camera, and (d) pinhole Faraday cup.

3.4.2. Faraday cup

A beam diagnostic probe (a Faraday cup) is used for measurements of the current. The Faraday cup is specially designed to function in a plasma environment. It consists of hole plates with hole sizes comparable to the Debye length, in order to prevent plasma from entering into the cup. The cup geometry and external circuitry are optimized to assure a fast time response (< 3 ns). A particle-in-cell code has been used to model the propagation of the intense ion beam and to design the diagnostic probe. The characteristics of the cup have been published elsewhere[21].

4. Beam compression experiment

4.1. Instrumental pulse timing

The longitudinal beam compression experiment depends on the simultaneous pulsing of Marx, quadrupoles, tilt core, plasma channel and plasma guns waveforms. All triggers for the system are generated from multiple DG-535 trigger generators which share a common terminal or

referring time, T_0. A computer triggers the first System DG-535 through a GPIB interface.

To align the peak of the plasma channel solenoid current with the peak in the magnet currents, the four magnets are triggered at 1.28 ms. This delay does not include the time-delay for the magnetic field to penetrate the beam pipe and is therefore not the peak of the magnetic field. The plasma source is then triggered at 1.92ms. This delay allows the plasma to be on for about 200 μs before the Marx is triggered.

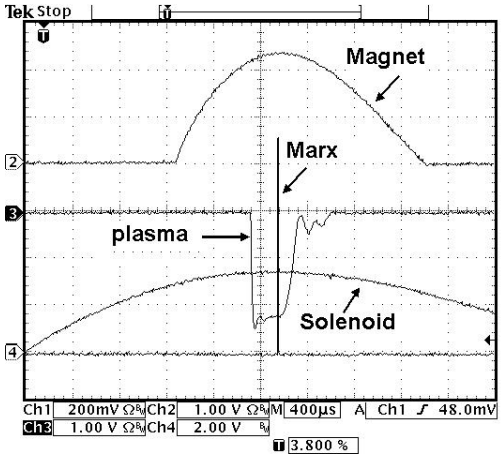

Fig. 7: Operational timing of the NDCX system including the pulse of the Marx, plasma plug, solenoid current for the plasma column, and quadrupoles.

The Marx is then fired at 2.149 ms at the peak of the plasma channel solenoid current, the peak of the magnet currents, and after the cathodic are plasma has been on for 200 μs. The crowbar is triggered at 2.16 ms to produce pulse from the Marx. This delay is dependent on the diagnostic used. The tilt core modulators M1-M6 are triggered together at 2.156 ms near the middle of the Marx voltage to produce the negative part of the tilt waveform. Individual modulator delay times and waveform accuracy have been considered. The tilt core modulators M7-M12 are triggered to produce the positive part of the tilt waveform. Individual modulator delay times and waveform accuracy have been considered. The reset circuits for the tilt core modulators are all triggered at T_0, so that the cores are reset before the modulators are triggered. The approximate timing of the waveforms has been verified on a oscilloscope. The fine tuning associated with measured cable delays is shown in Fig. 7.

4.2. Tilt cell waveform optimization

When the tilt voltage waveform was turned on, beam bunching was observed in the downstream diagnostic box. The degree of bunching, as well as the pulse shape, shown in Fig. 8, was clearly correlated with the voltage waveform, shown in Fig. 9. Theory specifies the ideal voltage waveform required to produce an exactly linear (versus z) velocity ramp [14, 15]. The induction module voltage waveform was optimized to obtain a rather close approximation to the ideal waveform as shown in Fig. 10 by varying the timing of the individual cores. Once we had the experimental waveform, the jitter ofthat waveform was measured. For 20 beam pulses using the waveform with 23kV charge and 80V reset, measurements showed that the tilt core had a jitter of 2 ns (± 1 ns).

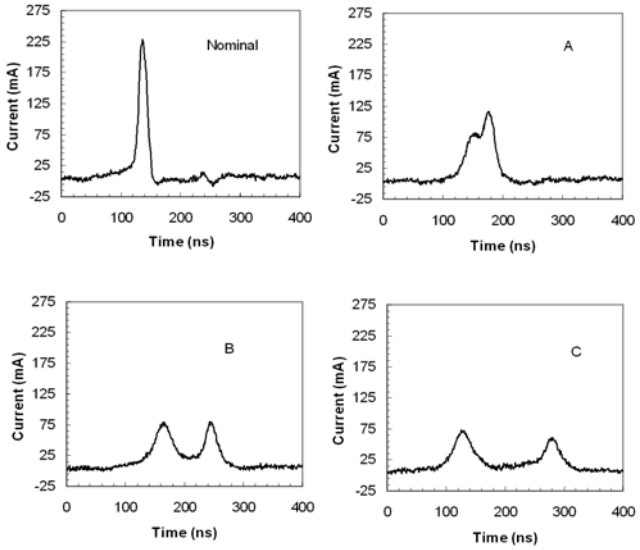

Fig.8: Neutralized drift-compressed beam current with the voltage waveforms in Fig.9.

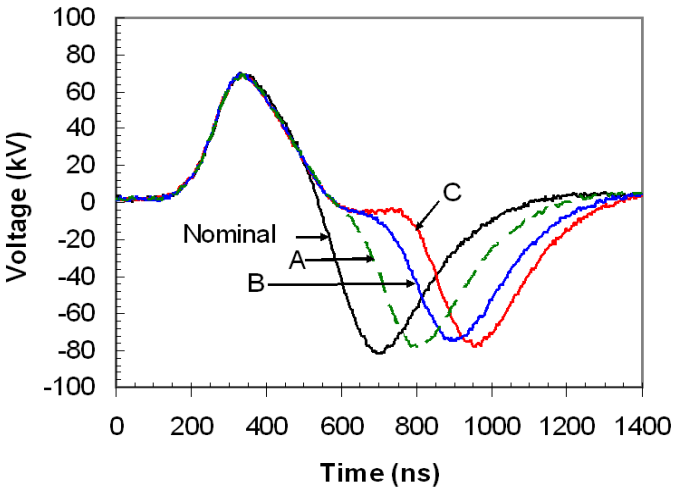

Fig.9: Induction module voltage waveforms produced by varying the timing of the modulators.

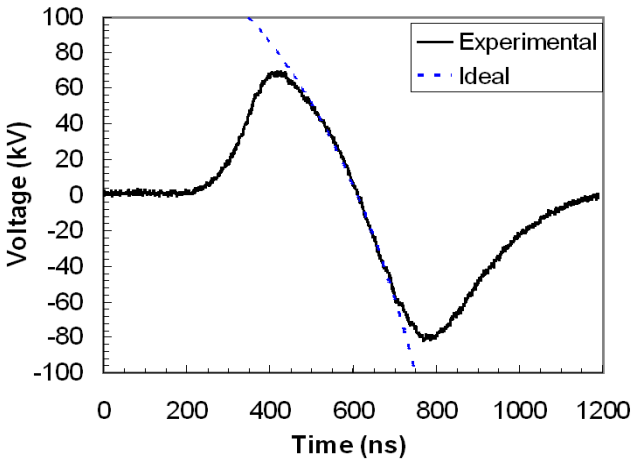

Fig. 10: Experimentally optimized and ideal induction module voltage waveforms.

4.3. Beam energy optimization

For a given voltage waveform, the position of maximal compression is changed as the beam energy is varied. A scan in beam energy demonstrates this behaviour and is shown in Fig. 11.

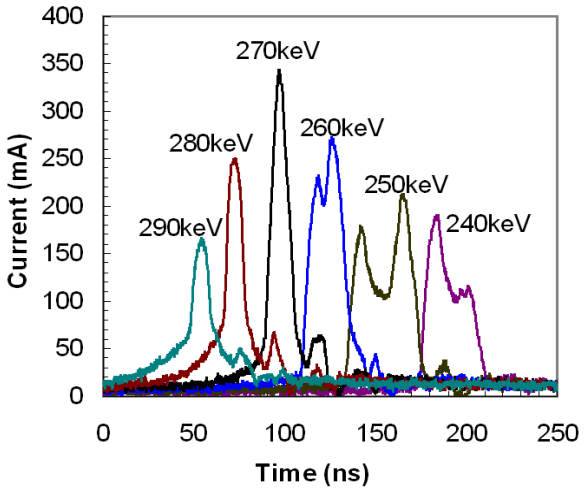

Fig. 11: Compressed beam current pulses using a nominal tilt core voltage waveform as the beam energy is varied.

4.4. Effective plasma density

The strong effects of neutralization are evident by comparing the compression ratio with the plasma turned on and off. Figure 12 shows that the peak current is significantly reduced when the plasma is turned off. LSP[22] simulations under similar conditions show qualitatively similar results. Note that the simulated beam energy and observing station do not exactly match those of the experiment.

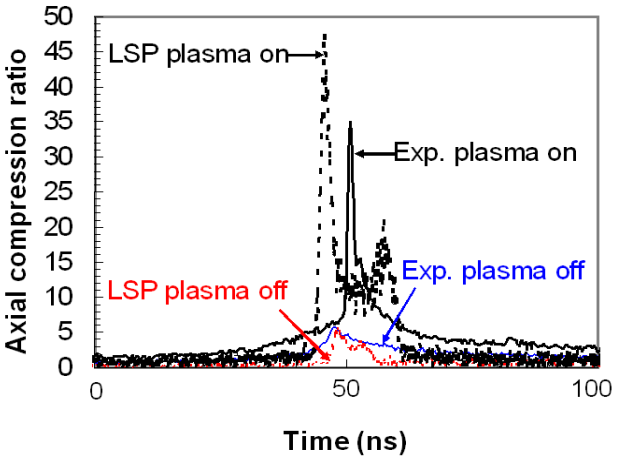

Fig. 12: Experimental data and LSP simulation of beam compression with neutralization (plasma source on) and without neutralization (plasma source off).

4.5. Maximum beam compression

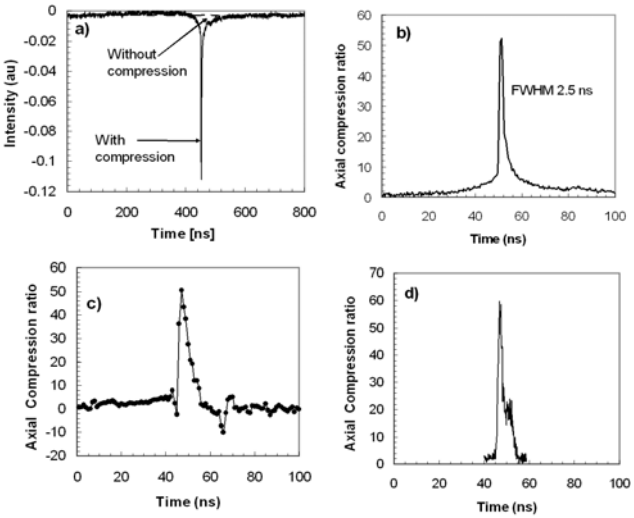

FIG. 13: (a) Measurements of beam signal using the phototube diagnostic for neutralized non-compressed, and neutralized compressed beams, (b) compression ratio obtained from the measurements using the phototube, (c) compression ratio obtained from measurements using the Faraday cup, and (d) LSP simulation for axial compression ratio under the experimental conditions.

The maximum compression is observed by fine tuning the beam energy to match the voltage waveform and precisely position the longitudinal focal point at the diagnostic location. This case is shown in Fig. 13. The

compression ratio of about 50, seen in Fig. 13(b), is obtained by taking the ratio of the signal with tilt voltage on (with compression) to the signal with tilt voltage off (without compression), see Fig. 13(a). A similar result is measured with the Faraday cup, see Fig. 13(c). LSP simulations under these experimental conditions predicted a peak compression ratio of 60 [Fig.13(d)] and indeed, a slightly different approach to processing the data indicates a factor of about 60.

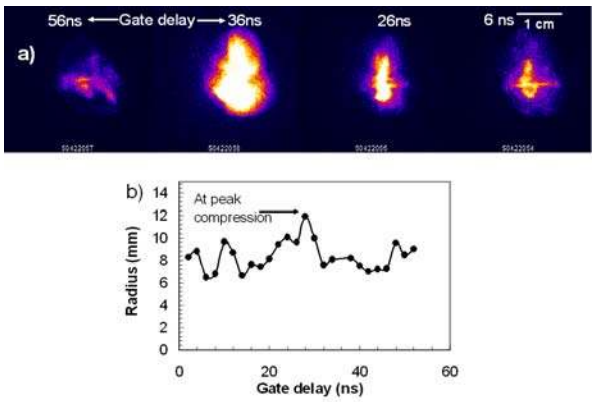

Fig. 14: Transverse images of neutralized longitudinal compressed beam: (a) optical profile, and (b) beam radius.

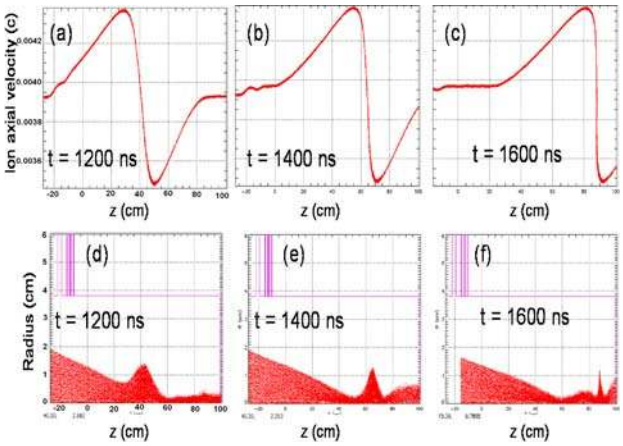

Fig. 15: The ion beam axial phase space (a)-(c) and configuration space (d)-(e) at 1200, 1400, and 1600 ns obtained from an LSP simulation. The neutralizing plasma extends for $z > -5$ cm.

In NDCX, optical imaging was deployed to measure the transverse beam size as a function of time during longitudinal compression. We were able to measure the images with a 1 ns time resolution. The measured spots in Fig. 14 for the 1-m beam focusing angle had roughly a 6-mm radius; while the simulation yields a 5-mm radius for a 13.5 m-rad angle. It was interesting to observe that the transverse spot size was larger at the point of maximal compression, as shown in Figs. 14(a) and 14(b). This feature was due to time-dependent defocusing effects occurring at the induction gap, and was also seen in LSP simulations, as shown in Fig.15.

4.6. Effect of drift length on compression

Theory predicts that the nature of the beam compression is strongly dependent on the drift length [14]. As the length is increased, the compression is more sensitive to the degree of neutralization. It is also more sensitive to the intrinsic longitudinal temperature of the ion beam. Finally, if there are any instabilities, e.g. two-stream, they may become evident with longer drift lengths. Although theory predicts two-stream effects to be benign, an experimental confirmation was deemed desirable.

For the above reasons, we have performed additional experiments with the plasma-filled drift length extended to two meters. We are able to recover the 50-fold compression in the 2-m experiment as shown in Fig. 16. The corresponding LSP simulation is also shown.

On the basis of this two-meter experiment we conclude that: 1) the degree of charge neutralization is sufficient to achieve 50 fold longitudinal compression while avoiding space-charge blow-up of the beam for the experimental configuration investigated; 2) the intrinsic longitudinal temperature is less than 1eV; and 3) no collective instabilities have been observed.

Transverse as well as longitudinal compression is required to achieve the high intensity required for high energy density physics and fusion applications, as mentioned earlier. Simulations indicate that the small spot sizes required for a fusion target [23,24] could be achieved with plasma neutralization [22, 25]. We have previously studied the effects of plasma neutralization [1-6] and are preparing for experimentally exploring simultaneous transverse and longitudinal compression.

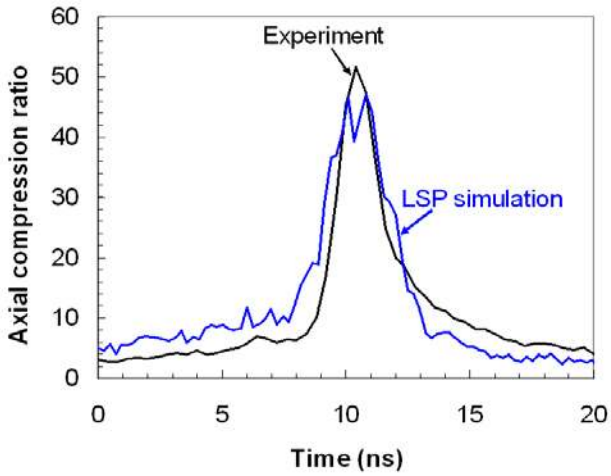

Fig. 16: Comparison of beam compression between experiment and LSP simulation for the 2-m long plasma column.

Acknowledgement:

This Research was supported by the U.S. Department of Energy under Contract No. DE-AC02-05CH11231 with the Lawrence Berkeley National Laboratory, Contract No. DE-AC02-76CH03073 with Princeton Plasma Physics Laboratory, and Contract No. DE-W-7405-Eng-48 with Lawrence Livermore National Laboratory for Heavy Ion Fusion Science (HIFS)-Virtual National Laboratory (VNL). We thank Dr. C. Celata and Dr. E. Lee for useful discussions and comments. Thanks also to Mr. D. L. Vanecek and all of the technical staff of the HIFS-VNL for useful technical assistance.

References:

[1] S. S. Yu et al., in *Proc. of the 2003 Particle Accelerator Conf.*, edited by J.Chew, (IEEE, 2003), p. 98.
[2] E. Henestroza, et al., Phys. Rev. ST Accel. Beams **7**, 083501 (2004).
[3] P. K. Roy et al., Phys. of Plasmas **11**, 2890 (2004).
[4] B. G. Logan et al., Nucl. Fusion **45**, 131 (2005).
[5] C. Thoma et al., Phys. of Plasmas **12**, 043102 (2005).
[6] P. K. Roy et al., Nucl. Instrum. Meth. Phy. Res. A **544**, 225 (2005).
[7] D. D.-M. Ho, S. T. Brandon and E. P. Lee, Particle Accelerators **35**, 15 (1991).
[8] T. Kikuchi, M. Nakajima, and K. Horioka, Phys. of Plasmas **9**, 3476 (2002).
[9] M. J. L. de Hoon, E. P. Lee, J. J. Barnard and A. Friedman., Phys. of Plasmas **10**, 855 (2003).
[10] H. Qin et al., Phys. Rev. ST Accel. Beams **7**, 104201 (2004).
[11] R. C. Davidson and H. Qin, Phys. Rev. ST Accel. Beams, **8**, 064201 (2005).
[12] W. M. Sharp et al., Nucl. Instrum. Meth. Phys. Res. A **544**, 398 (2005).
[13] W. M. Fawley et al., Phys. Plasmas **4**, 880 (1997).
[14] D. R. Welch et al., Nucl. Instrum. Meth. Phys. Res. A **544**, 236 (2005).
[15] C. Thoma et al., in *Proc. of the 2005 Particle Accelerator Conf.*, edited by C. Horak (IEEE, 2005), p.4006.
[16] P. K. Roy, S. S. Yu, E. Henestroza, A. Anders, F. M. Bieniosek, J. Coleman, S. Eylon, W. G. Greenway, M. Leitner, B. G. Logan and W. L. Waldron, D. R. Welch and C. Thoma, A. B. Sefkow, E. P. Gilson, P. C. Efthimion and R. C. Davidson, Physical Review Letters, **95**, (2005), pp. 234801.
[17] J. J. Barnard and S. M. Lund, "Intense Beam Physics, Space Charge, Halo, & Related Topic, LBNL report# 54926.
[18] A. Anders and G. Y. Yushkov, J. Appl. Phys. **91**, 4824 (2002).
[19] A. Anders and R. A. MacGill, Surf. Coat. Technol. **133-134**, 96 (2000).
[20] F. M . Bieniosek et al., Nucl. Instrum. Meth. Phy. Res. A **544**, 268 (2005).
[21] A. B. Sefkow, R. C. Davidson, P. C. Efthimion, and E. P. Gilson, S. S. Yu, P.K. Roy, F.M. Bieniosek, J. E. Coleman, S. Eylon, W. G. Greenway, E. Henestroza, J.W. Kwan, D. L. Vanecek, and W. L. Waldron, D. R. Welch, Phy. Rev. ST Accel. Beams, **9**, (2006) 052801.
[22] D. R. Welch et al., Nucl. Instrum. Meth. Phys. Res. A **464**, 134 (2001).
[23] S. S. Yu et al., Nucl. Instrum. Meth. Phy. Res. A **544**, 294 (2005).
[24] W. M. Sharp et al., Fusion Sci. Technol. **43**, 393 (2003).
[25] W. M. Sharp et al., Nucl. Fusion **44**, 221 (2004).